Spatial Distribution of Posterior Pole Choroidal Thickness by Spectral Domain Optical Coherence Tomography

Yanling Ouyang,[1] *Florian M. Heussen,*[1] *Nils Mokwa,*[1] *Alexander C. Walsh,*[1] *Mary K. Durbin,*[2] *Pearse A. Keane,*[3] *P. James Sanchez,*[4] *Humberto Ruiz-Garcia,*[1] *and Srinivas R. Sadda*[1]

Purpose. To study the spatial distribution of posterior pole choroidal thickness (CT) in healthy eyes using spectral domain optical coherence tomography (SD-OCT).

Methods. Fifty-nine eyes from 30 subjects with no retinal or choroidal disease were examined with high-definition (HD) OCT using macular volume cube scanning protocols. A randomly chosen subset also had multifield analysis performed (volume scans centered on and surrounding the optic nerve head [ONH]). CT was manually quantified using a validated reading center tool. For macular scans, mean CT was calculated for each Early Treatment Diabetic Retinopathy Study subfield. Compound posterior pole CT maps were also created through the alignment of OCT projection images. Regression analyses were used to evaluate the correlation between CT and axial length (AL), refractive error, age, sex, and ethnicity.

Results. Subfoveal CT was 297.8 ± 82.2 μm, which did not differ significantly from that of the inner macular subfields. CT was greatest in the superior outer subfield and thinnest in the nasal outer subfield. The most predictive models for macular CT included AL and/or age. Outside the macula, CT was thinnest inferonasal to the ONH.

Conclusions. CT demonstrates large variations between individuals, but also at different locations within the posterior pole; substantial choroidal thinning inferonasal to the ONH was demonstrated. CT appears to correlate more with distance from the optic nerve than from the fovea and, thus, in future studies, the ONH may serve as a better reference point than the foveal center for expressing or depicting regional CT variations. (*Invest Ophthalmol Vis Sci.* 2011;52:7019–7026) DOI:10.1167/iovs.11-8046

The choroid, a vascular meshwork between the retina and sclera, plays a major role in providing oxygen and nutrition to the outer layers of the retina.[1] In recent years, increased awareness of its role in ocular development and its known association with many diseases of the posterior pole have stimulated a renewed focus on understanding choroidal anatomy and physiology.[2] A number of methods, including histology[3] and ultrasonography,[4] have previously been used to quantify choroidal thickness (CT); however, the overall precision of these approaches is still lacking. Fortunately, the recent introduction of spectral domain optical coherence tomography (SD-OCT) and the description of "enhanced depth imaging" scanning protocols have afforded a new opportunity to improve the accuracy of quantitative choroidal assessment. As a result, changes in CT have now been studied using different OCT technologies over a wide range of ocular pathologies (e.g., glaucoma,[5] inherited retinal diseases,[6] high myopia,[7] central serous chorioretinopathy,[8] polypoidal choroidal vasculopathy,[9] neovascular age-related macular degeneration [AMD],[9] and Vogt Koyanagi Harada disease[10]).

Although the use of OCT has provided many new insights into choroidal morphology, to date there exists a notable disparity between the CT measurements obtained in different studies. For example, several studies on the cross-sectional variation of CT measurements in "normal" subjects have shown CT to be greatest at the fovea, with decreasing thickness more nasally than temporally.[9,11,12] Other results suggest that the foveal CT is thinner than the choroid superior to the fovea.[13] These discrepancies may arise due to the use of different image acquisition methodologies, a generally limited field of view for scanning, and inconsistencies in choosing the exact locations for repeated CT measurement. Regardless, the exact spatial distribution of CT changes in the macular region of human eyes remains unclear.

In addition, most OCT-derived studies have focused on assessment of CT in the macular region alone, examining the correlation between macular CT changes and disease expression. However, unlike the neurosensory retina, a complex and highly organized neural structure with the fovea as its unmistaken center, the choroid is a vascular layer with a potentially very different topography. Determination of choroidal spatial distribution may thus be difficult, and potentially inaccurate, in the context of macular scanning alone. In this report, we aim to address these issues by obtaining larger, two-dimensional (2D) maps of the spatial distribution of the choroid in the posterior pole and identifying its specific patterns in healthy volunteers using SD-OCT.

From the [1]Doheny Eye Institute and Department of Ophthalmology, Keck School of Medicine of the University of Southern California, Los Angeles, California; [2]Carl Zeiss Meditec, Dublin, California; the [3]National Institute for Health Research Biomedical Research Centre for Ophthalmology, Moorfields Eye Hospital National Health Service Foundation Trust and University College London Institute of Ophthalmology, London, United Kingdom; and [4]Washington University, St. Louis, Missouri.

Supported in part by Deutsche Forschungsgemeinschaft Grant He 6094/1-1, National Eye Institute Grants EY03040 and R01 EY014375, and grants from Research to Prevent Blindness and the Department of Health's National Institute for Health Research Biomedical Research Centre for Ophthalmology at Moorfields Eye Hospital and University College London Institute of Ophthalmology.

Submitted for publication June 13, 2011; revised July 19, 2011; accepted July 19, 2011.

Disclosure: **Y. Ouyang**, None; **F.M. Heussen**, None; **N. Mokwa**, None; **A.C. Walsh**, P; **M.K. Durbin**, Carl Zeiss Meditech (E); **P.A. Keane**, None; **P.J. Sanchez**, None; **H. Ruiz-Garcia**, None; **S.R. Sadda**, Heidelberg Engineering (C), Carl Zeiss Meditec (F), Optovue Inc. (F), Optos (F), P

Corresponding author: Srinivas R. Sadda, Doheny Eye Institute, 1450 San Pablo Street, Los Angeles, CA 90033; ssadda@doheny.org.

METHODS

Data Collection

In this study, 59 eyes from 30 normal volunteers were prospectively recruited from July 17, 2010 to October 6, 2010. Written informed consent was obtained from all subjects. Approval for data collection and analysis was obtained from the Institutional Review Board of the University of Southern California. The research adhered to the tenets set forth in the Declaration of Helsinki.

Information about age, sex, and race was gathered before clinical ophthalmic examination. All subjects underwent SD-OCT imaging as well as autorefraction and axial length (AL) measurement. SD-OCT scans were taken with both high definition (HD)-OCT (Cirrus software; Carl Zeiss Meditec, Dublin, CA) and a prototype SD-OCT (Carl Zeiss Meditec) incorporating a longer-wavelength light source (1050 nm) for enhanced choroidal penetration. For each device a volumetric OCT scanning protocol was used (128 B-scans $\times$ 512 A-scans). For each participant, both eyes were imaged, with image sets being centered on the fovea. A subset of randomly chosen eyes was also imaged after pupil dilation for multifield analysis. This subset of eyes had multiple SD-OCT volume scans taken from around the optic nerve head (ONH) (centered on the ONH, nasal to the ONH, temporal to the ONH, superior to the ONH, inferior to the ONH).

Grading Methodology

Raw OCT data were exported from the imaging instruments and imported into validated custom grading vector-based 3D imaging, modeling, and measurement software (3D-OCTOR; Able Software Corp., Lexington, MA). This software enables easy navigation of SD-OCT volume scans and manual boundary annotation of each B-scan or a subset of B-scans. Based on these boundaries, thicknesses and volumes can be calculated for each defined space by bilinear interpolation between the B-scans. Scans were considered to be gradable if the choroidal scleral junction was visible in at least 90% of B-scans. Scans from the HD-OCT system were reviewed first. If deemed ungradable due to incomplete visualization of the entire extent of the choroid, corresponding scans from the 1050-nm prototype SD-OCT were checked for improved choroidal visibility and graded accordingly. To validate that CT determined by the 1050-nm prototype and the HD-OCT could be used interchangeably for subsequent analyses, an inter-device reproducibility exercise was undertaken. Ten sets of volume OCT scans obtained using both devices were randomly selected and the CT was determined in a masked fashion and compared between devices.

To calculate CT maps, for images centered on the fovea, the foveola was manually identified by sequentially scrolling through the volume OCT B-scans. For scans centered on the optic nerve, the center of the ONH was manually identified using the OCT projection map and its coordinates were noted. All grading was performed using a dual-grader reading center protocol as previously described.[14] Disagreements between graders were resolved by open adjudication to yield a single final segmentation for each B-scan.

For retinal thickness calculation, we have previously demonstrated that not every B-scan in a dense (128 B-scans) volume cube needs to be segmented to generate an accurate retinal thickness map[15]; only a subset (32, or every fourth scan) of B-scans is sufficient.[15] It is unknown whether this observation generalizes to CT measurements. For this reason (i.e., to verify that the results were virtually identical), for the first five cases, the choroid was manually segmented on all 128 B-scans and the CT maps generated were then compared with maps generated using only every fourth B-scan (32 total). After this validation, for the remaining 54 cases the choroid was manually segmented in only every fourth B-scan (32 total) of the 128 B-scan volume cubes (Fig. 1).

Data Analysis

For all cases, the subfoveal CT was calculated. Then, based on the Early Treatment Diabetic Retinopathy Study (ETDRS) grid, the macula was divided into nine subfields: the superior outer macula (SOM), temporal outer macula (TOM), inferior outer macula (IOM), nasal outer macula (NOM), superior inner macula (SIM), temporal inner macula (TIM), inferior inner macula (IIM), nasal inner macula (NIM), and central subfield (CSM); in addition, three aggregate macular subfields were defined: "inner macular ring" (including SIM, TIM, IIM, and NIM), "outer macular ring" (including SOM, TOM, IOM, NOM), and "total macula" (including all nine subfields). Mean and SD of CT for each macular subfield were then calculated. The coefficient of variation (CV) of CT in each macular subfield was also calculated by dividing the SD from the mean.

For statistical analysis, one-way ANOVA and post hoc multiple comparisons were used to compare the CT in each single macular subfield. The correlation analyses of CT in all macular subfields with AL, refractive error, age, sex, and ethnicity, were also analyzed. Multiple regression analysis was performed to assess the influence of AL and age on CT. Bland Altman plots were used to assess intergrader agreement. A 95% range of agreement was defined as mean $\pm$ 2SD. The level of significance was set at $P < 0.05$. All analyses were performed using commercially available statistical software (Stata 10; StataCorp LP, College Station, TX).

In the five cases with 128 manually graded B-scans, the macular CT measurements were compared based on computation of every B-scan or every fourth B-scan, respectively, to evaluate for measurement inaccuracies due to increased interpolation between scans.

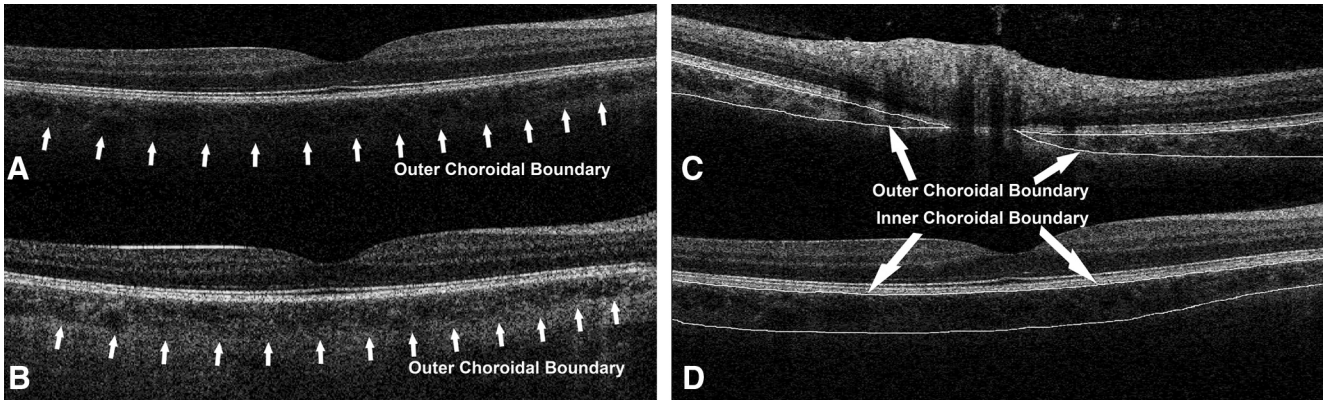

FIGURE 1. Grading of choroidal inner and outer boundaries. (**A**, **B**) Sample OCT B-scan from the same eye obtained with a regular 840-nm wavelength OCT (**A**) and a prototype 1050-nm wavelength OCT (**B**). The outer choroidal boundary (choroid scleral boundary) is much better visualized with the longer wavelength. (**C**, **D**) Examples of manual grading of both inner and outer choroidal boundaries as performed in our study.

Table 1. Demographics of Patients in the Study

Variable	Value
Patients/eyes	28/55
Sex (males/females)	14:14
Age, mean years ± SD (range)	32.85 ± 11.45 (20–68)
Refractive error, median diopters (range)	−0.50 (−8.0, +2.50)
Axial length, mean cm ± SD (range)	23.83 ± 1.33 (20.98, 26.41)
Race: Caucasian/Asian/Latino	14:11:3

Individual CT maps from each graded OCT image set were also obtained. Three-dimensional (3D) annotations (x = A-scan location, y = B-scan location, and z = CT) for each graded point from each set of OCT scans were first generated. For eyes with more than two gradable overlapping OCT scans, OCT projection maps were exported and registered using commercially available software (Adobe Photoshop CS3 Extended, version 10.0). For each eye, the x and y from each individual 3D annotation were converted to a new relative location based on the overlap of the projection maps to generate a composite 3D CT map. 3D CT maps were then created for all eyes that underwent multifield analysis.

In a separate analysis, a mean CT map covering a 6 × 6 mm area and centered on the fovea was generated based on all available OCT scans. Similarly, another map was created, but this time centered on the ONH. Patterns of CT distribution were compared between the two maps. Subsequently, the mean CT with distance from the ONH was plotted for all four quadrants by choosing the center of ONH as the origin of the axes.

Results

Characteristics of the Study Population

A total of 59 eyes from 30 subjects were imaged, among which 13 eyes from 13 subjects underwent multifield OCT examination. Of the macular scans, 51 eyes of 27 subjects were gradable from the regular HD-OCT data set. Of the remaining 8 eyes, 4 were gradable from the 1050-nm Zeiss prototype image sets. Despite using both OCT systems, 4 eyes remained ungradable due to poor visualization of the outer choroidal interface on either data set. After exclusion of the ungradable cases, 55 eyes from 28 subjects were included in the final analysis. The demographic characteristics of the normal cohort are summarized in Table 1.

A statistically significant correlation of AL with refraction was found with Pearson analysis (R^2 = 0.40, $P < 0.001$). Age did not correlate significantly with AL or refraction ($P > 0.05$, respectively).

Effect of Scan Density of CT

The absolute difference (mean ± SD) between CT values obtained using the subset of 32 B-scans and those obtained using all 128 B-scans was 4.1 ± 3.9 μm, with a range of 0 to 10.2 μm, whereas the relative error was between 0% and 6.1%, with a

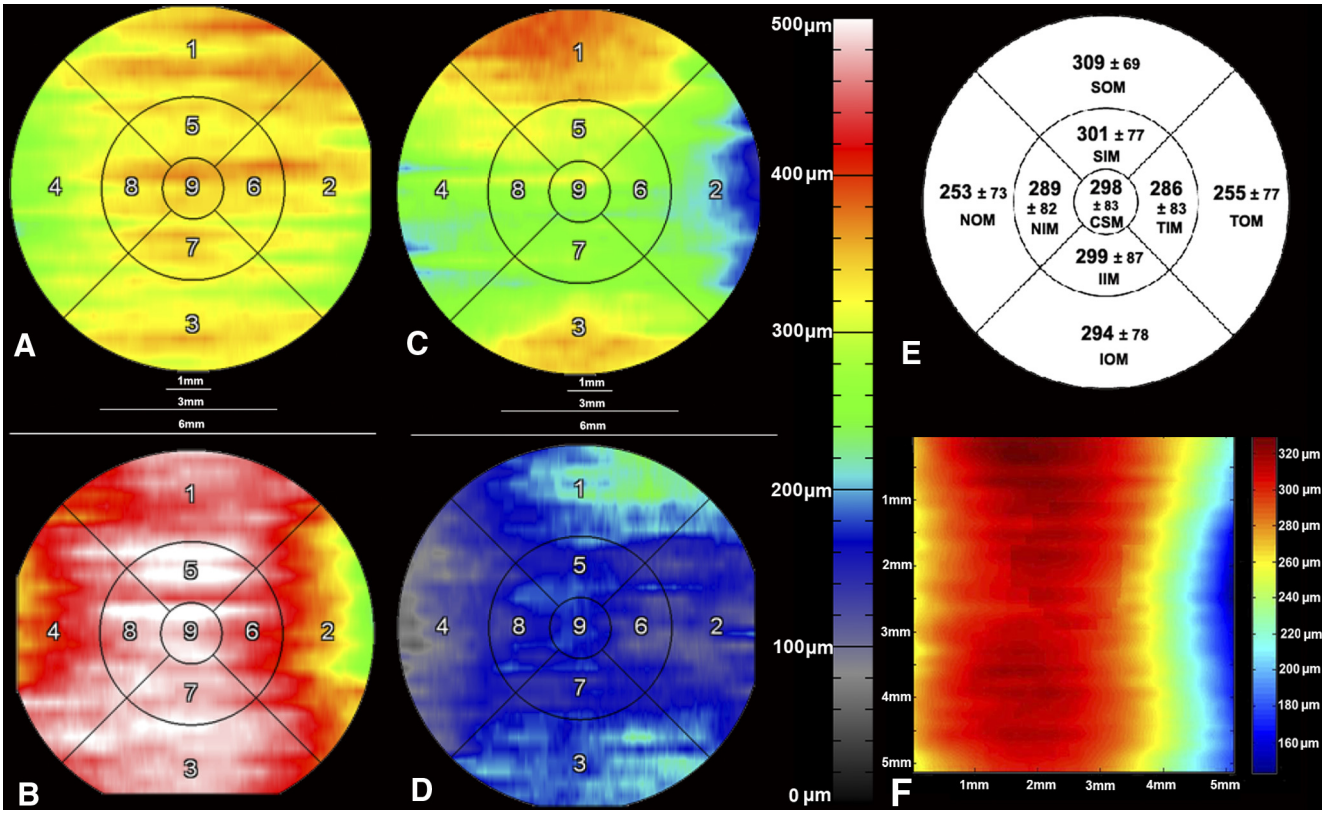

Figure 2. Choroidal thickness variations in the macula. (**A**–**D**) Individual choroidal thickness (CT) maps in an ETDRS grid derived from a 6 × 6 mm area centered on the fovea. (**A**) Left eye of a normal 29-year-old Asian female; AL = 23.72 cm, refraction = −1.50D. (**B**) Right eye of a normal 30-year-old Caucasian female; AL = 21.17 cm, refraction = +0.75 D. (**C**) Right eye of a normal 28-year-old Latino male; AL = 23.71 cm, refraction = +1.50 D. (**D**) Left eye of a normal 32-year-old Asian male; AL = 26.41 cm, refraction = −8.00 D. (**E**) Mean CT ± SD from all 55 eyes in an ETDRS grid derived from a 6 × 6 mm area centered on the fovea. (**F**) Mean CT of the representative locations in 6 × 6 mm macular area, centered on the fovea from 55 eyes. 1 = SOM, superior outer macula; 2 = TOM, temporal outer macula; 3 = IOM, inferior outer macula; 4 = NOM, nasal outer macula; 5 = SIM, superior inner macula; 6 = TIM, temporal inner macula; 7 = IIM, inferior inner macula; 8 = NIM, nasal inner macula; 9 = CSM, central subfield.

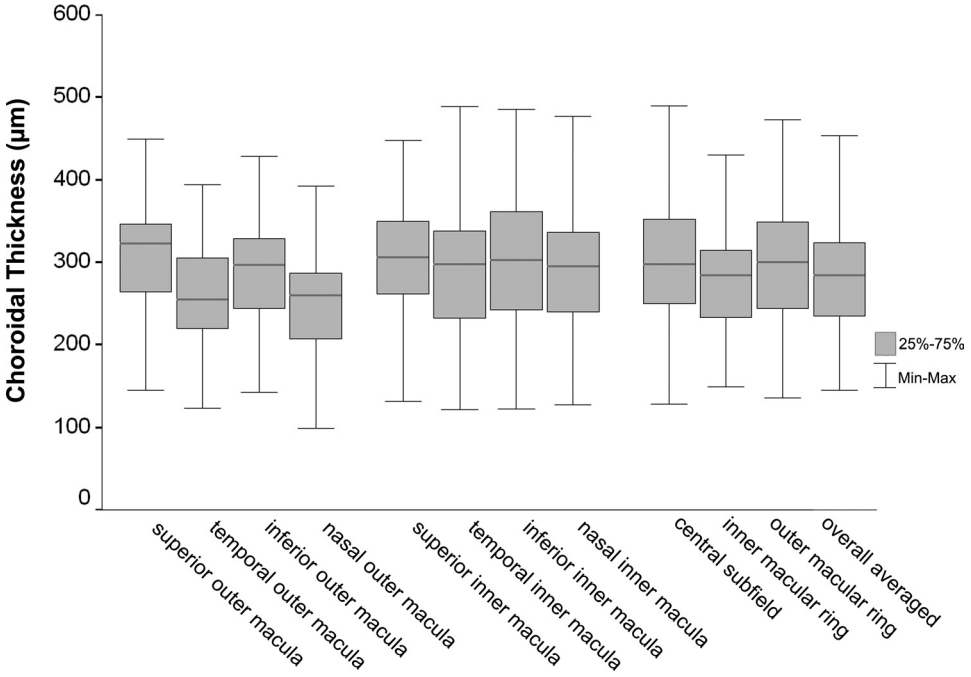

FIGURE 3. Box and whisker plots of choroidal thickness in each macular subfield. The *bottom* and the *top* of the box represent the 25th and the 75th percentiles, respectively, whereas the band near the middle of the box is the 50th percentile (the median). The ends of the *whiskers* represent the minimum and maximum of all the data.

mean of 1.5%. For individual subfields, the maximum difference was smallest in the NOM (2.5 μm) and largest in the IOM (10.2 μm). However, no significant difference between subfields was observed with respect to the effect of scan density.

CT in the Macular Region

Mean CT for each ETDRS macular subfield was generated from the 55 available eyes (Fig. 2). A box-and-whisker diagram of CT was also generated (Fig. 3). CT measurements differed significantly among the nine macular subfields [one-way ANOVA, $F(485,8) = 3.481$, $P = 0.001$]. Further post hoc multiple comparisons of Tukey's test indicated that CT in the SOM was significantly thicker than those in the NOM and TOM, whereas CT in SIM was significantly thicker than that in the NOM. Differences in CTs between TOM, TIM, NIM, IOM, IIM, SIM, and CSM were not statistically significant at $P < 0.05$ (Table 2). The CV values of CTs were lowest in SOM (22.3%) and SIM (24.8%) and highest in TIM (29.0%) and TOM (30.3%), with an average of 27.5% for all macular subfields.

Statistically significant correlations were found between mean CT in the various subfields and refraction ($P < 0.05$ in all subfields), as well as with AL ($P < 0.01$ in all subfields) (Table 3). Increasing AL or increasing myopia was associated with decreasing CT across all subfields. Mean CT showed a weak negative correlation with age in the SOM ($R^2 = 0.10$, $P = 0.021$) and IOM ($R^2 = 0.08$, $P = 0.035$), but not in the foveal subfield or the other macular subfields or rings ($P > 0.05$) (Table 3). No correlation of CT in any subfield or ring was observed for eye (left or right), sex, or ethnicity ($P > 0.05$ in all subfields).

TABLE 2. Tukey Post Hoc Comparisons of the Mean Choroidal Thickness across Nine ETDRS Macular Grid Subfields

		Mean Choroidal Thickness (μm) Subset for alpha = 0.05		
Macular Subfield	**Eyes (*n*)**	**1**	**2**	**3**
Nasal outer	55	253.2		
Temporal outer	55	254.8	254.8	
Temporal inner	55	285.8	285.8	285.8
Nasal inner	55	288.9	288.9	288.9
Inferior outer	55	294.0	294.0	294.0
Central subfield	54	297.5	297.5	297.5
Inferior inner	55	298.6	298.6	298.6
Superior inner	55		301.1	301.1
Superior outer	55			308.8
P		0.067	0.056	0.841

P value is significant at the 0.05 level (two-tailed).

Multiple linear regression analyses were performed to determine the most predictive variables for mean averaged CT in all macular subfields. Since a statistically significant correlation was found between AL and refraction, refraction was excluded from the regression analyses. As a result, AL and age were tested as the two possible independent predictors for the linear regression model. The models were statistically significant subfoveally and in all macular subfields ($P < 0.005$, Table 4A). AL ($P \leq 0.001$ in all subfields) correlated significantly with CT subfoveally and in all subfields. Age was a significant predictor of CT subfoveally and in most subfields ($P < 0.05$) but not in TOM and TIM ($P > 0.05$, respectively). For the regression model for individual subfields, taking CSM as an example, CT in CSM decreased 1.95 μm for each year of age or 31.96 μm for each 1-mm increase in AL ($R^2 = 0.34$, $P < 0.001$; Table 4B).

A representative map of mean CT from all cases in the central 6 × 6 mm is shown in Figure 2F. CT did not vary in a consistent or steady fashion in all directions with increasing eccentricity from the fovea, a finding consistent with observations from the individual mean macular CT maps.

CT in the ONH Region

The mean CT map centered on the ONH, within a 6 × 6 mm area, was generated using the 13 available eyes that had ONH scans performed (Fig. 4A). A consistent pattern was observed in all cases, with the choroid thickest superior to the ONH, followed by temporal and nasal to the ONH, with the thinnest part of the choroid inferonasal to the ONH.

Posterior Pole CT

CT maps derived from a montage of all available posterior pole data (covering both fovea and ONH) were also generated in a

TABLE 3. Pearson Correlation Analyses of Mean Choroidal Thickness with Age, Refraction, and Axial Length

	Age		Refraction		Axial Length	
Macular Subfield	***R***	***P***	***R***	***P***	***R***	***P***
Subfoveal	−0.234	0.089	0.336	0.013	−0.485	0.001
Central subfield	−0.234	0.088	0.333	0.014	−0.504	0.001
Superior outer	−0.311	0.021	0.280	0.038	−0.403	0.007
Temporal outer	−0.142	0.301	0.350	0.009	−0.515	<0.001
Inferior outer	−0.285	0.035	0.276	0.042	−0.530	<0.001
Nasal outer	−0.219	0.109	0.316	0.019	−0.445	0.003
Superior inner	−0.259	0.056	0.333	0.013	−0.431	0.004
Temporal inner	−0.191	0.163	0.350	0.009	−0.535	<0.001
Inferior inner	−0.239	0.078	0.329	0.014	−0.502	0.001
Nasal inner	−0.243	0.074	0.314	0.019	−0.504	0.001
Inner macular ring*	−0.265	0.051	0.341	0.011	−0.525	<0.001
Outer macular ring†	−0.240	0.078	0.342	0.011	−0.508	0.001
Total macula	−0.259	0.056	0.341	0.011	−0.523	<0.001

P value is significant at the 0.05 level (two-tailed).

* Including superior inner, temporal inner, inferior inner, and nasal inner subfield, but not central subfield.

† Including superior outer, temporal outer, inferior outer, and nasal outer subfield.

subset of 13 eyes as a means of examining CT variation over a larger posterior region (examples shown in Figs. 5A, 5B). A consistent pattern was observed, with the choroid relatively thicker in the macula and in the superior aspect of the ONH, and thinner in the inferonasal portion of ONH. The choroid in eyes with myopia was generally thinner than that in emmetropic eyes.

Choosing the center of ONH as the center of the axis, and dividing the posterior pole into four quadrants (based on ONH center), a plot of the mean CT in the four quadrants as a function of the distance to the ONH center was also generated (Fig. 4B). CT in the various quadrants showed a consistent relationship with distance from the ONH, peaking at an approximate distance of 5 to 6 mm from the ONH center, and decreasing more peripherally.

TABLE 4. Multiple Linear Regression Analyses of Axial Length (AL) and Age as the Two Possible Predictors of Mean Choroidal Thickness

A. Overall Model

Macular Subfield	Significant Predictors	R^2	*F*	*P*
Subfoveal	AL, Age	0.32	9.60	<0.001
Central subfield	AL, Age	0.34	10.45	<0.001
Superior outer	AL, Age	0.34	10.12	<0.001
Temporal outer	AL	0.30	8.57	0.001
Inferior outer	AL, Age	0.41	14.13	<0.001
Nasal outer	AL, Age	0.28	7.58	0.002
Superior inner	AL, Age	0.30	8.49	0.001
Temporal inner	AL	0.34	10.32	<0.001
Inferior inner	AL, Age	0.34	10.26	<0.001
Nasal inner	AL, Age	0.35	10.93	<0.001
Inner macular ring*	AL, Age	0.35	10.73	<0.001
Outer macular ring†	AL, Age	0.39	12.82	<0.001
Overall averaged	AL, Age	0.38	12.36	<0.001

B. Examples for Parameter Estimates

Macular Subfield	Coefficient	SE	*t*	*P*
Total macula				
Constant	1025.32	155.81	6.58	<0.001
Age	−1.85	0.70	−2.65	0.011
AL	−28.44	6.36	−4.48	<0.001
Central subfield				
Constant	1128.05	187.89	6.00	<0.001
Age	−1.95	0.84	−2.33	0.025
AL	−31.96	7.66	−4.17	<0.001

P value is significant at the 0.05 level (two-tailed).

* Including superior inner, temporal inner, inferior inner, and nasal inner subfield, but not central subfield.

† Including superior outer, temporal outer, inferior outer, and nasal outer subfield.

Interdevice Reproducibility

The absolute difference (mean ± SD) between mean CT values across all macular subfields obtained using the HD-OCT and the prototype long-wavelength SD-OCT was 11.7 ± 9.1 μm, with a range of 0.3 to 38.8 μm.

Intergrader Reproducibility

The Bland Altman analysis indicated that the 95% limits of agreement between the two graders ranged from −13.3 to 10.7 μm (mean, 1.3 μm) for CTs of all macular subfields (Fig. 6). Similar levels of agreement were observed when considering individual subfields.

DISCUSSION

In recent years, a number of studies have measured CT using "enhanced depth" OCT scanning protocols, or using prototype long-wavelength OCT devices.[7–13,16–23] However, for the most part, these studies have measured CT at various points along a single, horizontal, and/or vertical OCT B-scan running through the fovea.[7–13,17–21] As a result, quantitative information regarding the spatial distribution of CT is limited. In the present study, we address this issue through the manual segmentation of OCT volume scans, allowing us to generate CT measurements for each subfield of the widely used ETDRS grid and to evaluate 2D CT maps. Furthermore, by obtaining OCT volume scans outside the macula (i.e., centered on, and surrounding, the ONH), and combining their projection images, we were able to more accurately analyze the spatial distribution of CT across the posterior pole.

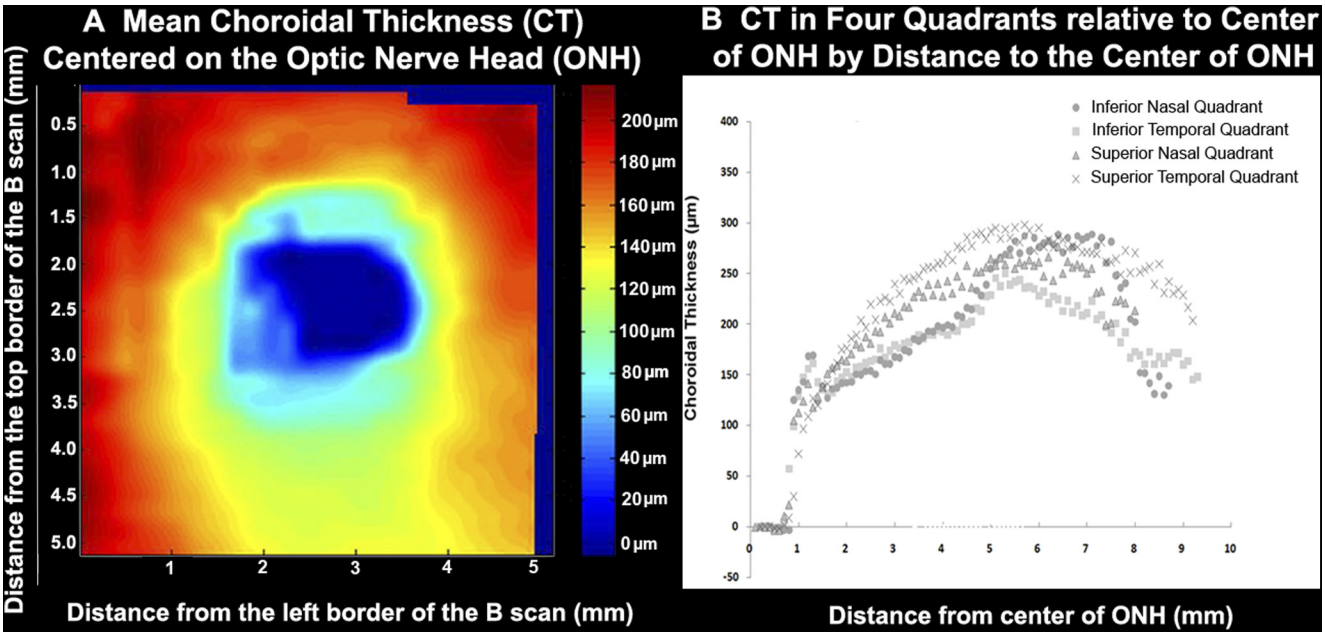

Figure 4. CT in the optic nerve head region. (**A**) Mean CT map derived from a 6 × 6 mm area, centered on the ONH, generated from 13 eyes (*left border*: temporal aspect of macula; *right border*: nasal aspect of macula). (**B**) Consistent relationship with distance from the ONH, peaking at an approximate distance of 5 to 6 mm from the ONH center, and decreasing more peripherally.

In our study, the subfoveal CT measured 297.8 ± 82.2 μm, thicker than that reported by Manjunath et al. (272 ± 81 μm)[17] and Margolis and Spaide[11] (287 ± 76 μm), but thinner than that observed by Esmaeelpour et al.[13] (315 ± 106 μm) and Ikuno et al.[12] (354 ± 111 μm). In addition, a study by Ikuno et al.,[19] assessing the reproducibility of CT measurements in healthy subjects, reported values of 292.7 ± 77.3 μm using a long-wavelength OCT prototype, and 283.7 ± 84.1 μm using "enhanced depth" imaging (i.e., results very similar to those described herein). Recently, investigators have begun to consider not only CT in the foveal center, but also CT in the various subfields of the ETDRS grid.[22,23] Significant differences were observed, however, in the CT values among studies. For example, whereas mean CT was reported to be 202.6 ± 83.5 μm by Hirata et al.,[23] it was determined to be 355 ± 73 μm by Agawa et al.[22] In our study, we also determined the CT in various ETDRS macular subfields (although the optimum grid or layout for expressing the distribution of CT values is unknown, we used the commonly used ETDRS grid to facilitate measurement comparison between different macular regions). The results of our study suggest that the choroid is thickest, on average, in the superior outer ETDRS subfield and thinnest, on average, in the nasal outer ETDRS field. No statistically significant differences in CT were found among the remaining ETDRS subfields.

Previous studies evaluating CT, using both OCT derived and histologic findings, have found statistically significant negative correlations between CT and age (i.e., decreases in CT with increases in age).[3,11,12] Other studies have also reported an apparent lack of correlation between CT and age.[13] In our study, macular CT was found to correlate significantly with age, but only for the superior outer and inferior outer subfields. We speculate that the relatively narrow age range of subjects evaluated in the present study (32.85 ± 11.45 years) precluded the detection of stronger correlations. Nonetheless, using multiple regression analyses, we found that the most significant models for the prediction of macular CT incorporated AL and/or age. In particular, we found that CT in the central macular subfield decreased 1.95 μm for each additional year of age, or 31.96 μm for each 1-mm increase in AL, findings comparable to those previously reported by Margolis and Spaide.[11] Away from the fovea, increasing age or AL was

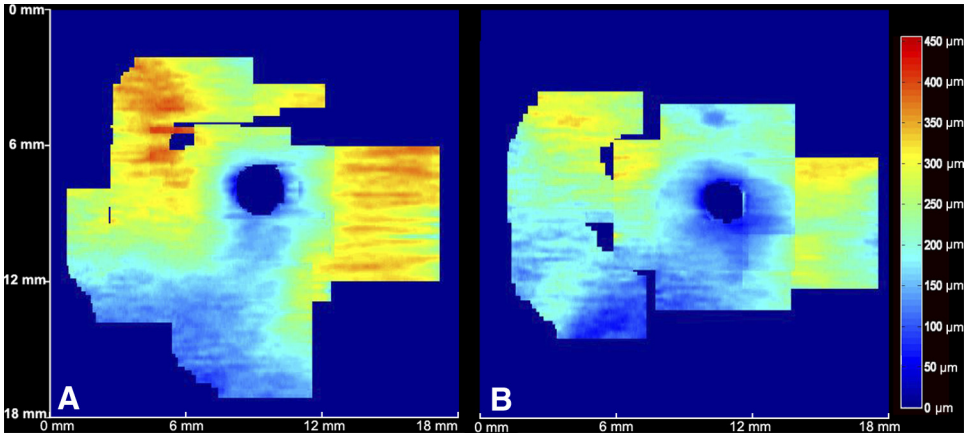

Figure 5. Individual posterior pole CT maps. (**A**) Mean CT map derived from representative locations in the posterior pole, in the left eye of a normal 29-year-old female. (**B**) Mean CT map derived from representative locations in the posterior pole, in the left eye of a normal 26-year-old male.

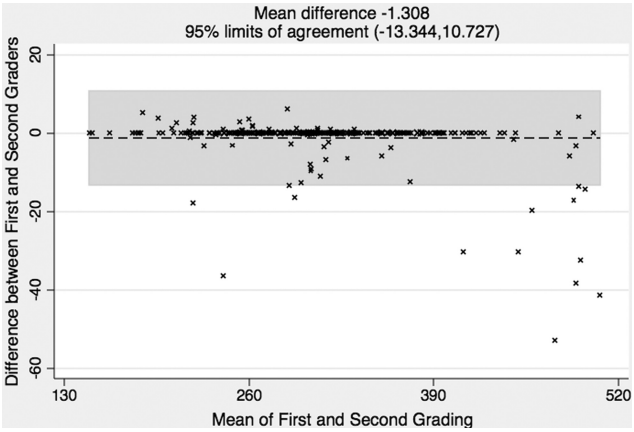

FIGURE 6. Bland Altman plot of intergrader agreement on CT measurements for all macular subfields together between the two graders. The × symbol represents a set of first and second grading for the same CT measurement. Each of the measurements is then represented on the graph by assigning the mean of the two gradings as the *x*-axis value, and the difference between the two gradings as the *y*-axis value. The overall mean difference is shown as a dashed line; the 95% limits of agreement lie within the *gray box*. The variation is relatively small for this data set.

associated with more dramatic CT decreases in the inferior macula versus those seen superiorly. Similarly, increasing age or AL was associated with greater CT decreases in the temporal versus the nasal macula.

Overall, the pattern of macular CT variation observed in our study differed from that previously reported.[7,11,12,17] For example, although there was a reduction in thickness nasally and temporally, the thickness appeared to increase superiorly and was relatively unchanged inferiorly. In addition, the choroid appeared to show more thinning nasally compared with that temporally. More specifically, macular CT did not appear to change in a consistent manner at varying eccentricities from the foveal center (Fig. 2F). However, when the center of the ONH was chosen as the reference point, a more consistent spatial relationship was seen (Figs. 4A, 4B).

The choroid immediately adjacent to the optic nerve ("peripapillary") appeared thin, but increased in thickness with eccentricity from the nerve in all directions (up to a certain point), except inferiorly. This spatial relationship appeared consistent in the posterior pole across all individuals. Thus, in future studies, the ONH center may serve as a better reference point than the foveal center for expressing or depicting regional variations in CT.

The observation of a relatively thinner choroid inferior to the optic nerve is perhaps not surprising and is consistent with previous studies.[12,13] Ikuno et al.,[12] for example, found prominent thinning in the inferior aspect of myopic eyes. They further speculated that the inferior choroid would be thinner even in nonmyopic eyes. Relative depigmentation and atrophy inferior to the optic nerve is common in myopes (who already have a thin choroid to begin with), and may be a reflection of this apparent inferior choroidal thinning. Although it remains unclear why the inferior choroid demonstrates such prominent thinning, we favor the theories put forward by Ikuno et al.,[12] that both a vascular water shed zone and the embryonic location of optic fissure closure may be responsible. A failure of closure of the optic fissure is commonly known to clinicians as a coloboma, which is typically located in the inferonasal quadrant of the globe.[24] Atypical colobomas can also occur without an embryonic fissure defect.[24] Our finding in normal subjects with consistent choroidal thinning inferonasal to the ONH could be interpreted as a remnant of normal embryological development, perhaps conceptualized as a "relative " coloboma that all healthy eyes express.

Our study has a number of limitations. First, this is a relatively small normative case series that does not include a wide age distribution. Second, due to the lack of an effective automated grading algorithm, CT measurements were obtained from exhaustive manual grading of OCT B-scans. This prevented complete segmentation of 128 B-scans in all cases and ultimately limited the size of the study cohort. However, the mean difference in CT values obtained using 32 B-scans versus 128 B-scans, in the initial five analyzed eyes, was 4.1 $\pm$ 3.9 μm (range, 0–10.2 μm), a difference that is unlikely to be clinically meaningful. In addition, good intergrader reproducibility was also confirmed in our study and increases our confidence in the thickness measurement. Third, CT measurements were obtained in some cases using different devices (Cirrus OCT vs. 1050-nm OCT). Although interdevice variability could potentially confound our analyses, comparison of CT measurements derived from two OCT devices yielded a difference of 11.7 $\pm$ 9.1 μm, differences that were in the range of intergrader reproducibility, and less than the observed variation in CT between regions. Fourth, a number of factors with a potential influence on absolute CT, such as diurnal variation, blood pressure, other systemic factors, and hydration status, for example, were not controlled for. Despite this, since the principal goal of this study was to evaluate relative regional variations, this failure may be less relevant. A final potential limitation is that the use of an ETDRS grid may not constitute the optimal design for the analysis of regional CT variations. This grid, however, is well recognized and may facilitate comparisons with thickness measurements of adjacent structures such as the neurosensory retina. New measurement grids, perhaps centered on the optic nerve, should be considered for future CT studies.

In summary, the findings from our study suggest that CT measurements in ETDRS macular subfields appear thickest in the superior outer macula and thinnest in the nasal outer macula, without significant differences among the remaining subfields. The regression models using AL and/or age as the predictors for macular CT were statistically significant. Macular CT appears to decrease with increasing AL and/or age. Significant variations in CT were noted among individuals, but consistent/characteristic patterns of spatial variation were observed, particularly when considering CT changes relative to the optic nerve center. Thus, in future studies, the ONH may serve as a better reference point than the foveal center for expressing or depicting regional CT variations.

References

1. Bron AJ, Tripathi RC, Wolff E, Tripathi BJ. *Wolff's Anatomy of the Eye and Orbit*. 8th ed. London: Chapman & Hall Medical; 1998.
2. Nickla DL, Wallman J. The multifunctional choroid. *Prog Retinal Eye Res.* 2010;29:144–168.
3. Ramrattan RS, van der Schaft TL, Mooy CM, de Bruijn WC, Mulder PG, de Jong PT. Morphometric analysis of Bruch's membrane, the choriocapillaris, and the choroid in aging. *Invest Ophthalmol Vis Sci.* 1994;35:2857–2864.
4. Hung LF, Wallman J, Smith EL. Vision-dependent changes in the choroidal thickness of macaque monkeys. *Invest Ophthalmol Vis Sci.* 2000;41:1259–1269.
5. Kubota T, Jonas JB, Naumann GO. Decreased choroidal thickness in eyes with secondary angle closure glaucoma. An aetiological factor for deep retinal changes in glaucoma? *Br J Ophthalmol.* 1993;77:430–432.
6. Yeoh J, Rahman W, Chen F, et al. Choroidal imaging in inherited retinal disease using the technique of enhanced depth imaging optical coherence tomography. *Graefes Arch Clin Exp Ophthalmol.* 2010;248:1719–1728.

7. Fujiwara T, Imamura Y, Margolis R, Slakter JS, Spaide RF. Enhanced depth imaging optical coherence tomography of the choroid in highly myopic eyes. *Am J Ophthalmol.* 2009;148:445–450.
8. Maruko I, Iida T, Sugano Y, et al. Subfoveal choroidal thickness after treatment of central serous chorioretinopathy. *Ophthalmology.* 2010;117:1792–1799.
9. Chung SE, Kang SW, Lee JH, Kim YT. Choroidal thickness in polypoidal choroidal vasculopathy and exudative age-related macular degeneration. *Ophthalmology.* 2011;118:840–845.
10. Maruko I, Iida T, Sugano Y, et al. Subfoveal choroidal thickness after treatment of Vogt-Koyanagi-Harada disease. *Retina*. 2011;31:510–517.
11. Margolis R, Spaide RF. A pilot study of enhanced depth imaging optical coherence tomography of the choroid in normal eyes. *Am J Ophthalmol.* 2009;147:811–815.
12. Ikuno Y, Kawaguchi K, Nouchi T, Yasuno Y. Choroidal thickness in healthy Japanese subjects. *Invest Ophthalmol Vis Sci.* 2010;51:2173–2176.
13. Esmaeelpour M, Povazay B, Hermann B, et al. Three-dimensional 1060-nm OCT: choroidal thickness maps in normal subjects and improved posterior segment visualization in cataract patients. *Invest Ophthalmol Vis Sci.* 2010;51:5260–5266.
14. Ouyang Y, Keane PA, Sadda SR, Walsh AC. Detection of cystoid macular edema with three-dimensional optical coherence tomography versus fluorescein angiography. *Invest Ophthalmol Vis Sci.* 2010;51:5213–5218.
15. Sadda SR, Keane PA, Ouyang Y, Updike JF, Walsh AC. Impact of scanning density on measurements from spectral domain optical coherence tomography. *Invest Ophthalmol Vis Sci.* 2010;51:1071–1078.
16. Ehrlich JR, Peterson J, Parlitsis G, et al. Peripapillary choroidal thickness in glaucoma measured with optical coherence tomography. *Exp Eye Res.* 2011;92:189–194.
17. Manjunath V, Taha M, Fujimoto JG, Duker JS. Choroidal thickness in normal eyes measured using Cirrus HD optical coherence tomography. *Am J Ophthalmol.* 2010;150:325–329.e1.
18. Maruko I, Iida T, Sugano Y, Saito M, Sekiryu T. Subfoveal retinal and choroidal thickness after verteporfin photodynamic therapy for polypoidal choroidal vasculopathy. *Am J Ophthalmol.* 2011;151:594–603.e1.
19. Ikuno Y, Maruko I, Yasuno Y, et al. Reproducibility of retinal and choroidal thickness measurements in enhanced depth imaging and high-penetration optical coherence tomography. *Invest Ophthalmol Vis Sci.* 2011;81:1–23.
20. Ikuno Y, Tano Y. Retinal and choroidal biometry in highly myopic eyes with spectral-domain optical coherence tomography. *Invest Ophthalmol Vis Sci.* 2009;50:3876–3880.
21. Imamura Y, Fujiwara T, Margolis R, Spaide RF. Enhanced depth imaging optical coherence tomography of the choroid in central serous chorioretinopathy. *Retina.* 2009;29:1469–1473.
22. Agawa T, Miura M, Ikuno Y, et al. Choroidal thickness measurement in healthy Japanese subjects by three-dimensional high-penetration optical coherence tomography. *Graefes Arch Clin Exp Ophthalmol.* In press.
23. Hirata M, Tsujikawa A, Matsumoto A, et al. Macular choroidal thickness and volume in normal subjects measured by swept-source optical coherence tomography. *Invest Ophthalmol Vis Sci.* 2011;52:4971–4978.
24. Hartnett ME, Trese M, Capone A Jr, Keats BJB, Steidl SM, eds. *Pediatric Retina: Medical and Surgical Approaches*. Philadelphia: Lippincott Williams & Wilkins; 2005:10–11.